Supporting Online Material for

Three-dimensional Super-resolution Imaging by Stochastic Optical Reconstruction Microscopy

Bo Huang, Wenqin Wang, Mark Bates and Xiaowei Zhuang

The Supporting Online Material includes

Materials and Methods

1. Sample preparation

Characterization of the 3D localization of individual fluorophores. To characterize the 3D localization accuracy of photo-switchable probes, streptavidin molecules (Invitrogen) were doubly labeled with the photo-switchable Alexa 647 fluorophore (Invitrogen) and the activator dye Cy3 (GE Healthcare) by incubating the protein with amine-reactive dyes following the suggested protocol from the manufacturers. Unreacted dye molecules were removed by gel filtration using a Nap-5 column (GE Healthcare). The labeling ratio was characterized by a UV-Vis spectrophotometer and the absorption spectrum indicated a labeling ratio of ~2 Cy3 and ~0.1 Alexa 647 per streptavidin molecule. The labeled streptavidin was then immobilized onto the surface of a glass flow chamber assembled from a glass slide and a #1.5 coverglass. Slides and coverglasses were cleaned by sonicating in 1 M potassium hydroxide for 15 min, followed by extensive washing with MilliQ water and drying with compressed nitrogen. The labeled streptavidin sample was injected into the flow chamber to allow the streptavidin to adsorb on the surface directly or through a biotin-streptavidin linkage on the biotinylated bovine serum albumin (BSA) coated surface. To generate the calibration curve for *z* localization measurement, Alexa 647-labeled streptavidin or quantum dots (Protein A coated Qdot 655, Invitrogen) were also used. The singly labeled streptavidin were immobilized to the chamber surfaces in a similar manner as the Cy3 and Alexa 647 doubly labeled streptavidin and the quantum dots were immobilized directly to the surface by nonspecific binding.

Bead imaging. To make 200 nm polystyrene beads coated with photo-switchable fluorophores, the coverglass surface was first coated with streptavidin by flowing 0.25 mg/mL unlabeled streptavidin solution into the flow chamber as described above and then rinsed with phosphate buffered saline (PBS). Next, 200 nm diameter biotinylated polystyrene beads (Invitrogen) were added to the chamber to allow immobilization on the surface. Finally 3 μg/mL streptavidin labeled with Cy3 and Alexa 647, with a labeling ratio of ~2 Cy3 and ~0.1 Alexa 647 per protein, was flowed in to coat the surface of the biotinlylated beads. During this procedure, some fluorescent streptavidin also adsorbed nonspecifically onto the coverglass surface. The flow chamber was then rinsed with PBS to remove free streptavidin molecules in solution.

Immunofluorescence imaging of cells. BS-C-1 cells were plated in 8-well chambered coverglasses (LabTek-II, Nalgene Nunc) at a density of 40k cells per well. After 16 – 24 hours, the cells were fixed using 3% paraformaldehyde and 0.1% glutaraldehyde in PBS for 10 min, and then treated with 0.1% sodium borohydride for 7 min to reduce the unreacted aldehyde groups and fluorescent products formed during fixation. The sodium borohydride solution was prepared immediately before use to avoid hydrolysis. The fixed sample was then washed three times with PBS, and permeabilized in blocking buffer (3% w/v BSA, 0.5% v/v Triton X-100 in PBS) for 15 min.

Microtubules were stained with mouse monoclonal β-tubulin antibodies (ATN01, Cytoskeleton) for 30 min and then goat anti-mouse secondary antibodies for 30 min. The secondary antibodies were doubly labeled with amine-reactive Alexa 647 and Cy3 and the labeling stoichiometry was characterized to be ~4.0 Cy3 and ~0.4 Alexa 647 per antibody. Three washing steps using 0.2% w/v BSA and 0.1% v/v Triton-X100 in PBS were performed after each staining step.

For staining clathrin by direct immunofluorescence, mouse monoclonal anti-clathrin heavy chain (clone X22, ab2731, Abcam) and anti-clathrin light chain (clone CON.1, C1985, Sigma-Aldrich) were used simultaneously. Both antibodies were labeled with ~ 1.0 Cy3 and ~1.0 Alexa 647 per antibody. The sample was stained for 30 min, washed three times with PBS and used immediately for STORM imaging.

We note that STORM immunofluorescence imaging can work well at a wide range of dye-labeling ratios. We typically chose a labeling ratio of ≥ 1 activator (Cy3 in this case) per antibody to ensure that the majority of antibodies had activators. On the other hand, when more than one photo-switchable reporter (Alexa 647 in this case) were attached to amino acid residues within close proximity on the same antibody, the reporter-reporter interaction can result in a significantly lower rate of switching off. Our previous characterization indicates that the off rate of two reporters separated by 2 nm was ~ 5 times slower than that of a single reporter whereas the two reporters separated by 7 nm have a comparable off rate as that of an isolated reporter (*S1*). Therefore, we typically chose a dye/protein ratio of ≤ 1 for the reporter to minimize this effect.

STORM imaging buffer. Buffer solutions in the samples were replaced with an imaging buffer immediately before STORM data acquisition. The imaging buffer contained 50 mM Tris, pH 7.5, 10 mM NaCl, 0.5 mg/mL glucose oxidase (G2133, Sigma-Aldrich), 40 μg/mL catalase (106810, Roche Applied Science), 10% (w/v) glucose and 1% (v/v) β-mercaptoethanol (*S1*).

2. STORM imaging procedure

Optical Setup. All STORM imaging experiments were performed on an inverted optical microscope (Olympus IX-71). Two solid state lasers were used as the excitation source: a 657 nm laser (RCL-200-656, Crystalaser) for exciting the photo-switchable reporter fluorophore (Alexa 647) and switching it to the dark state; and a 532 nm laser (GCL-200-L, Crystalaser) for reactivating the Alexa 647 in an activator (Cy3)-facilitated manner (*S1, S2*). The two lasers were combined and coupled into an optical fiber (P3-630A-FC-5, Thorlabs). The fiber output was collimated and focused onto the back focal plane of a high numerical aperture oil immersion objective (100× UPlanSApo, NA 1.4, Olympus) through the back port of the microscope. A translation stage allowed both laser beams to be shifted towards the edge of the objective so that the emerging light from the objective reached the sample at a high incidence angle near but not exceeding the critical angle of the glass-water interface. This excitation scheme allowed fluorophores within a few micrometers from the surface to be excited and reduced the background fluorescence from the solution (S3). The fluorescence emission was collected by the same objective and filtered by a polychroic mirror (z458/514/647rpc, Chroma), a band pass filter (HQ710/70m, Chroma) and a long pass filter (HQ665LP, Chroma). The filtered emission was then imaged onto an EMCCD camera (Ixon DV897DCS-BV, Andor) through a pair of relay lenses with a weak cylindrical lens (1 m focal length) inserted in between.

To stabilize the microscope focus during data acquisition, the reflected red excitation laser from the glass-water interface was directed onto a quadrant photodiode by a reflective prism at the back port of the microscope. The quadrant photodiode read the position of the reflected laser, which was sensitive to the distance between the coverglass surface and the objective. This information was then fed back to a *z*-positioning piezo stage (NanoView-M, MadCity Labs) by software to correct for the *z*-drift in the microscope focus. This "focus lock" system was capable

of maintaining the focus position within 40 nm for the duration of STORM data acquisition. Residual drift in z was corrected during data analysis, as described below.

Image acquisition. In STORM data acquisition, a relatively strong imaging/deactivation laser (~40 mW at 657 nm) and a relatively weak activation laser (< 2 μW at 532 mm) were applied to the sample simultaneously. The simultaneous illumination with both the activation and deactivation lasers resulted in the stochastic switching of the reporter fluorophores between the fluorescent and dark states. A strong imaging/deactivation laser power was chosen to ensure high emission intensity and a rapid switching off rate, and the relatively weak activation laser was chosen to ensure that the fraction of activated fluorophores at any given time was sufficiently low so that they were optically resolvable. The EMCCD camera acquired the images continuously at a frame rate of 20 Hz to obtain a "STORM movie".

3. Calibration of *z*-localization

In order to derive the z coordinates from the widths of the single molecule images, we generated calibration curves as shown in Fig. 1B. We performed calibration experiments in three ways: 1. Alexa 647 labeled streptavidin was adsorbed on the coverglass surface at a low density such that individual streptavidin molecules were resolvable from each other. The β-mercaptoethanol in the imaging buffer was replaced with 2 mM Trolox so that blinking of the fluorophore was suppressed (*S4*). The fluorescence images of individual streptavidin molecules were recorded while scanning the sample stage in z at a constant rate with the piezo stage; 2. Quantum dots were adsorbed onto the coverglass. A solution of 1% β-mercaptoethanol in PBS was used as the imaging buffer to suppress the blinking of quantum dots (*S5*). The fluorescence images of individual quantum dots were acquired while scanning the sample stage in z. 3. Cy3-Alexa 647 labeled streptavidin was adsorbed on the coverglass surface with high density. The measurement was performed in the same way as during STORM data acquisition except that the sample was scanned slowly in z at a constant rate. Photoactivation events in a small area (usually 8 μm × 4 μm) within the view field were used for measuring the calibration curve. All three measurements produced similar calibration curves.

Fluorescent peaks in each image frame of a calibration experiment were fit with an elliptical Gaussian function

$$G(x,y) = h\exp\left(-2\frac{(x-x_0)^2}{w_x^{\,2}} - 2\frac{(y-y_0)^2}{w_y^{\,2}}\right) + b$$

where h is the peak height, b is the background, (x_0, y_0) is the center position of the peak, and w_x and w_y stand for the widths of the image (point spread function, PSF) in the x and y directions, respectively. At the same time, we read out the z position of the corresponding molecule from the z trajectory of the piezo stage. The w_x and w_y values as a function of z were then fit to a modified form of a typical defocusing curve:

$$w_{x,y}(z) = w_0\sqrt{1+\left(\frac{z-c}{d}\right)^2 + A\left(\frac{z-c}{d}\right)^3 + B\left(\frac{z-c}{d}\right)^4}$$

where w_0 is the PSF width when a molecule is at the focal plane, c is the offset of the x or y focal plane from the average focal plane, d is the focus depth of the microscope, and A and B are coefficients of higher order terms to correct for the non-ideality of the imaging optics. The average focal plane is defined such that a fluorophore positioned in this plane has an image PSF

with equal widths in the x and y directions, thus generating a spherical image. We note that these fitting curves were generated to facilitate the automated z-localization when the measured w_x and w_y values were compared with the calibration curve to search for the corresponding z position. The exact functional form used for the fitting curve was unimportant as long as the curves fit the measured calibration data with sufficient precision.

4. STORM image analysis

The STORM data were analyzed in a similar manner as described previously (*S1*) but now with the additional z-dimension information derived from the shape of the image of individual activated fluorophores. Fluorescent peaks in each image frame of the STORM movie were identified by fitting local maxima with an elliptical Gaussian function to deduce the peak height h', the centroid position in the two lateral dimensions, x_0' and y_0', and the peak widths in the two lateral dimensions, w_x' and w_y'. Applying a threshold to the peak height (h'), width ($\sqrt{w_x' w_y'}$) and ellipticity (w_x'/w_y'), we rejected peaks too weak, too wide or too skewed to yield satisfactory localization accuracy and to avoid overlapping images of multiple fluorophores. If the center positions of identified peaks in consecutive frames were spatially separated by less than one pixel, they were considered as originating from the same molecule during one photoactivation event. All images from the same photoactivation event of the same fluorophore in different frames were averaged and a second fit to an elliptical Gaussian function was performed to deduce the refined center positions x_0 and y_0, and widths w_x and w_y. The area of the image used for the second fit was determined by the peak widths obtained in the initial fit.

After the second fit, the calibration curve was searched to find a z_0 point that best matched the measured widths w_x and w_y obtained from the fit. This search was performed automatically by minimizing the distance in the $w_x^{1/2}$ - $w_y^{1/2}$ space:

$$D = \sqrt{\left(w_x^{1/2} - w_{x,\mathrm{calib}}^{1/2}\right)^2 + \left(w_y^{1/2} - w_{y,\mathrm{calib}}^{1/2}\right)^2}$$

It can be shown by simulation and by an analytical treatment that using the square root of the widths slightly improves the accuracy of z localization in the search procedure as compared to using the widths directly. Activation events with a minimum distance D larger than a preset threshold indicated that the image was distorted, most likely caused by more than one molecule located in close proximity and photoactivated in the same image frame. These events were rejected from further analysis. This procedure allowed the 3D position (x_0 , y_0 and z_0) of each activated fluorophore to be obtained and in this manner the 3D STORM image was constructed.

When performing 3D STORM measurements of biological samples in an aqueous imaging buffer supported by glass substrates using an oil immersion objective, the mismatch of indices of refraction between glass (n = 1.515) and the imaging buffer (n = 1.35 for 10% glucose solution) need be considered. This index of refraction mismatch effectively shifts the apparent z position of an object away from the glass surface. Within a few micrometers from the surface, it was previously shown that this refractive-index-mismatch induced magnification of the z-distance can be treated as a constant and that the magnification factor is equal to 1.26 for the objective and refractive indices used in our imaging condition (objective: NA = 1.4, glass: n = 1.515 and buffer: n = 1.35) (*S6*). This small magnification effect was corrected accordingly in our z-localization analysis by rescaling all z values, obtained from direct comparison with the calibration curve, by a factor of 1/1.26 = 0.79.

Due to aberrations in the imaging optics, the PSF may become asymmetric when a fluorophore is out of focus, and as a result, the center of its image may deviate slightly from the actual lateral position of the fluorophore. This causes an apparent tilting distortion in the 3D image. The average tilt was typically no more than 4 degrees in our experiments and can be corrected by pre-calibration of the tilt profile if necessary.

An important factor that affects the localization accuracy is the sample stage drift during the image acquisition time, including both drift in *x*-*y* plane and drift in the *z* direction. In our setup, a focus lock was installed to minimize *z*-drift, but a residual drift of ~ 40 nm was present. The drift can be corrected using two methods as we have previously shown (*S1*). One method involves adding fiducial markers (fluorescent beads) to track the drift of the sample and subtracting the movement of the markers during image analysis (*S1*). The other method uses the correlation function of the image for drift correction (*S1*). Here we exploited the second method to correct for the *x*, *y* and *z* drift. A STORM movie was divided in time into equal-period segments and a STORM image was constructed from each movie segment. The correlation functions between the image in the first segment and all subsequent segments were then calculated and the centroid positions of the correlation functions were determined. Interpolations based on these centroid positions were used to generate a curve of the drift as a function of time for each imaging frame. This drift was then subtracted from the localizations and all localizations at different time points were included to generate the drift corrected STORM image. We note that this correction method only works for still images of fixed samples. For images that are time dependent, such as live cell images, the fiducial marker method is more suitable.

Supporting Figures

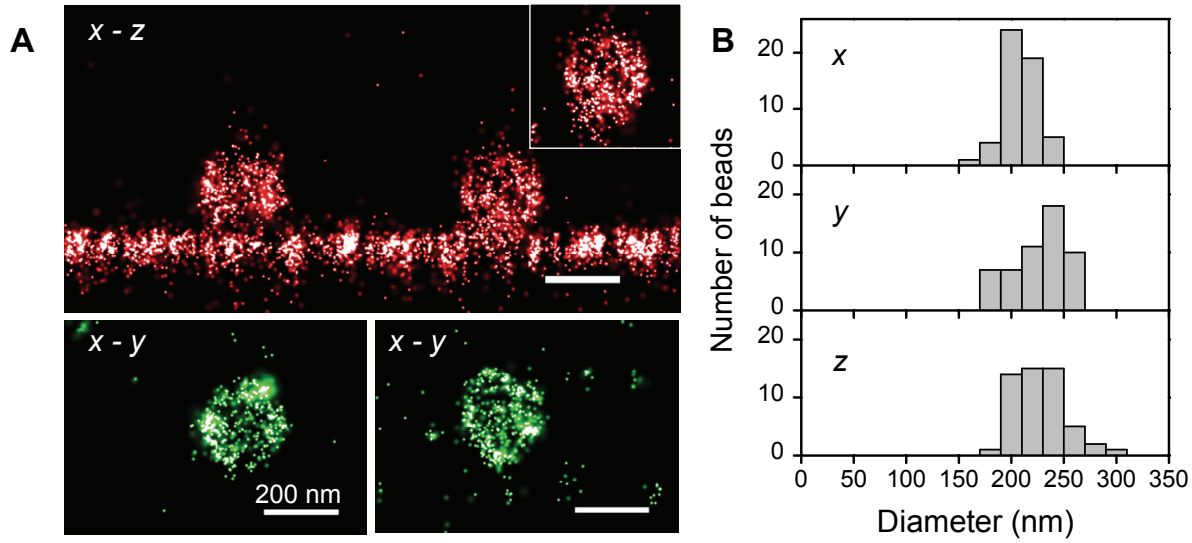

Fig. S1. Three-dimensional STORM images of 200 nm diameter beads coated with Cy3 and Alexa 647 doubly labeled streptavidin. **(A)** The upper panel shows the *x*-*z* projection of two beads within an area of 1.7 μm (*x*) × 10 μm (*y*) on the glass surface. The surface is defined by a line of localizations underneath the beads, resulting from streptavidin molecules nonspecifically adsorbed to the glass surface. Although the nonspecifically adsorbed streptavidins were only sparsely distributed on the surface, a large area projection results in an almost continuous line of localizations. Inset shows the *x*-*z* projection of a small volume (400 nm × 400 nm × 400 nm) surrounding the right bead, where only a few nonspecifically adsorbed streptavidin molecules were present. The two lower panels show the *x*-*y* projection of the two beads, together with localizations from a few non-specifically adsorbed streptavidin molecules. The slight deviation from a round shape may be in part due to the imperfect streptavidin coating and/or the intrinsically non-ideal bead shape. **(B)**. Distribution of the bead diameters in the *x*, *y* and *z* directions. To determine the diameters in an objective manner, we assumed that the streptavidin molecules were coated uniformly on the bead surface. Such a 3D uniform distribution on a spherical surface, when projected onto any of the *x*, *y* and *z* axes, should follow a 1D uniform distribution. The width of the 1D distribution in the *x*, *y* or *z* directions provides a measure of the diameter of the bead along the *x*, *y* or *z* axis, respectively. We further take advantage of the relation between the width (*d*) and the standard deviation (SD_{uniform}) of a uniform distribution, i.e. $SD^2_{\text{uniform}} = d^2/12$ and the relation between our measured standard deviation SD_{measure} and the SD_{uniform} value of the real uniform distribution considering finite localization accuracy ($SD_{\text{localization}}$), i.e. $SD^2_{\text{measure}} = SD^2_{\text{uniform}} + SD^2_{\text{localization}}$. From the independently measured localization accuracies ($SD_{\text{localization}}$) as shown in Fig. 1C, and the SD_{measure} of the projected distribution of the 3D bead image in the *x*, *y* and *z* directions, we deduced the diameters (*d*) of the beads along the *x*, *y* and *z* axes. The diameter distributions of 53 measured beads are shown here and the average diameters are 210 ± 16 nm, 226 ± 25 nm, and 228 ± 25 nm (mean ± SD) in the *x*, *y* and *z* directions, respectively. The measured diameters are quantitatively similar to the manufacturer's suggested diameter (200 nm) for the beads. The slight increase may be in part due to the finite thickness of the streptavidin coating.

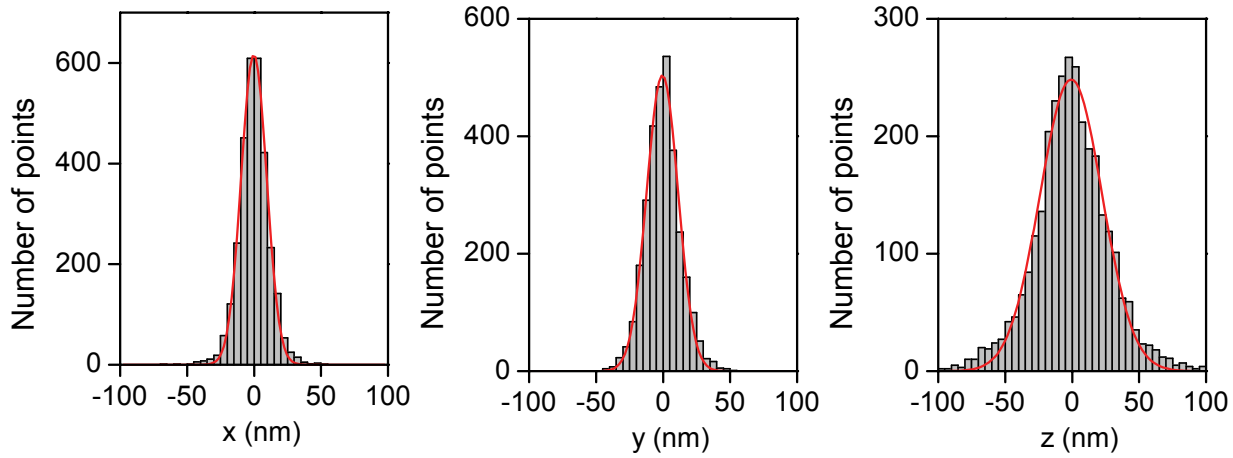

Fig. S2. Localization accuracy for 3D STORM images of the cell. The localization accuracy was determined from point-like objects in the cell, which appeared as small clusters of localizations away from any discernable microtubule filaments. Shown here is the spatial distribution of localizations within these point-like clusters in the *x*, *y* and *z* dimensions. The histogram of localizations was generated by aligning 202 clusters by their centers of mass, with each cluster containing ≥ 8 localizations. Fitting the histograms with Gaussian functions gave standard deviations of 9 nm, 12 nm, and 23 nm in the *x*, *y* and *z* directions, respectively. The corresponding FWHM values were 22 nm, 28 nm and 55 nm.

References:

S1. M. Bates, B. Huang, G. T. Dempsey, X. Zhuang, *Science* **317**, 1749 (2007).
S2. M. Bates, T. R. Blosser, X. Zhuang, *Phys. Rev. Lett* **94**, 108101 (2005).
S3. B. X. Cui *et al.*, *Proc. Natl. Acad. Sci., USA* **104**, 13666 (2007).
S4. I. Rasnik, S. A. McKinney, T. Ha, *Nat. Math.* **3**, 891 (2006).
S5. S. Hohng, T. Ha, *J. Am. Chem. Soc.* **126**, 1324 (2004).
S6. A. Egner, S. W. Hell, *Handbook of Biological Confocal Microscopy*. J. Pawley, Ed. (Springer, New York, 2006), pp. 404.

Supporting Movie Caption

Supporting Movie S1. The 3D presentation of microtubules shown in Figs. 2C-E. The viewing angle is rotated here to show different perspectives. The scale bar is 200 nm.